Frontiers in Bioscience Landmark

Front. Biosci. (Landmark Ed) **2025**; 30(1): 26796
https://doi.org/10.31083/FBL26796

Original Research

The Formation and Features of Massive Vacuole Induced by Nutrient Deficiency in Human Embryonic Kidney Cells

Dakang Sun[1,*], Xinye An[2], Yanli Cheng[3]

[1]Medical Research Center, Binzhou Medical University Hospital, 256603 Binzhou, Shandong, China
[2]Laboratory of Clinical Medicine, Binzhou Medical University Hospital, 256603 Binzhou, Shandong, China
[3]Department of Cardiovascular Medicine, Binzhou Medical University Hospital, 256603 Binzhou, Shandong, China
*Correspondence: sdkaaa@163.com (Dakang Sun)

Academic Editor: Margarita M Ivanova
Submitted: 30 September 2024 Revised: 14 November 2024 Accepted: 21 November 2024 Published: 17 January 2025

Abstract

Background: Cellular vacuolization is a commonly observed phenomenon under physiological and pathological conditions. However, the mechanisms underlying vacuole formation remain largely unresolved. **Methods**: LysoTracker Deep Red probes and Enhanced Green Fluorescent Protein-tagged light chain 3B (LC3B) plasmids were employed to differentiate the types of massive vacuoles. By confocal microscopy, lysosome-like massive vacuoles (LysoTracker Deep Red^{+}), autophagosome-like massive vacuoles (LC3B-enhanced green fluorescent protein (EGFP^{+})), and autolysosome-like massive vacuoles (LC3B-EGFP^{+} LysoTracker Deep Red^{+}) in starved HEK293T cells were observed. **Results**: In this study, we demonstrated that nutrient deficiency can induce the formation of massive vacuoles that appear highly electron-lucent in HEK293T cells. Additionally, these massive vacuoles, resulting from nutrient depletion, can originate from various organelles, including small vacuoles, autophagosomes, lysosomes, and autolysosomes. We found that massive vacuoles could form through two primary mechanisms: the accumulation of small vacuoles into larger vacuoles or the fusion of homogeneous or heterogeneous vacuoles. Further analysis revealed that the membranes of massive vacuoles, regardless of origin, were composed of a bilayer membrane structure. As the volume of the massive vacuoles increased, the cytoplasm and nucleus were displaced toward the periphery of the cells, leading to the formation of signet ring-like cells. Interestingly, we provided evidence that complete massive vacuoles or autophagosome-like massive vacuoles can be released and exist independently outside HEK293T cells. **Conclusions**: Nutrient deprivation induces the formation of heterogeneous, massive vacuoles in human embryonic kidney cells, some of which contribute to the development of signet ring cells, while others lead to extracellular vacuole formation.

Keywords: cellular vacuolization; massive vacuole; nutrient deficiency; signet ring like cells

1. Introduction

Cellular vacuolization is a morphological phenomenon observed in mammalian cells both *in vivo* and in culture [1,2]. The role of vacuoles in mammalian cells is often underestimated. It is important to recognize that cellular vacuolization serves as an adaptive, survival response to environmental changes; however, it can also contribute to cell death [3,4]. Methuosis, a specific form of cell death, occurs when cells excessively accumulate fluid through macropinocytosis [5]. This process can lead to the accumulation of late endosomes in the cytoplasm, and cytoplasmic vacuolation may persist for several days [6,7].

Cellular vacuolization is frequently observed in mammalian cells following exposure to bacterial or viral pathogens, as well as various inductive stimuli [8–10]. Both bacterial protein toxins and viral capsid or envelope proteins can induce cytoplasmic vacuolization [3,11,12]. In infected epithelial cells, human papillomavirus (HPV) can lead to the formation of multiple perinuclear vacuoles. Monel *et al.* [13] demonstrated that the Zika virus can induce extensive cytoplasmic vacuolization in human epithelial cells, astrocytes, and primary skin fibroblasts. Acute pancreatitis (AP) is a severe inflammatory disorder of the exocrine pancreas, which can induce not only dysregulation of digestive enzyme production but also cytoplasmic vacuolization [14]. Moreover, procaine and other drugs have been reported to induce vacuolization in various cell types [15–17]. Abamectin is widely used for its strong insecticidal and anthelmintic activities. It can induce large vacuoles in Sertoli and spermatogenic cells by electron microscopy examinations [18]. In addition, late endosomes can undergo vacuolization when treated with a phosphatidylinositol 3-kinase inhibitor in certain cells [19].

Autophagy can induce cellular vacuolization, which may reflect specific characteristics of this process [20,21]. Autophagosomes are cellular compartments formed under nutrient-deficient conditions and other pathological states [22]. Autophagy begins with the sequestration of cytoplasmic organelles within double membranes, followed by the generation of autolysosomes through the fusion of autophagosomes with lysosomes [23]. Autophagosomes are relatively small, with a diameter of 0.5–2 µm, similar to the size of mammalian lysosomes, which are approximately 0.5 µm in diameter [24]. However, autolysosomes can expand

significantly, sometimes filling the cytoplasm with a diameter of up to 10 µm, as observed under microscopy.

Recently, we investigated the formation process of massive autophagic vacuoles in HEK293T cells overexpressing the autophagosomal protein enhanced green fluorescent protein-microtubule associated protein light chain 3B (EGFP-LC3B) under nutrient-deficient conditions using confocal microscopy. Notably, we observed significant heterogeneity in these massive vacuoles under starvation conditions, raising the question of whether autolysosomes are the sole form induced to form massive vacuoles under starvation conditions. To differentiate the types of massive vacuoles, we employed LysoTracker Deep Red probes and EGFP-tagged LC3B plasmids. Consequently, by confocal microscopy, we observed lysosome-like massive vacuoles (LysoTracker Deep Red$^+$), autophagosome-like massive vacuoles (LC3B-EGFP$^+$), and autolysosome-like massive vacuoles (LC3B-EGFP$^+$ LysoTracker Deep Red$^+$) in starved HEK293T cells. Additionally, we examined the formation process and characteristics of these different types of massive vacuoles.

2. Materials and Methods

2.1 Plasmids and Reagents

The pEGFP-LC3B (human) vector was obtained from Wuhan Miaoling Bioscience & Technology (Wuhan, China), while the pEGFP-N3 vector was sourced from CLONTECH Laboratories, Inc. (Mountain View, CA, USA). LysoTracker Deep Red was procured from Thermo Fisher Scientific (L12492, Waltham, MA, USA), and Earle's balanced salt solution (EBSS) was purchased from Gibco (1854705, Waltham, MA, USA). 4′,6-diamidino-2-phenylindole (DAPI) was acquired from Sigma (D9542, St. Louis, MO, USA).

2.2 Cell Culture and Starvation Treatment

HEK293T cells were cultured in Dulbecco's Modified Eagle Medium (DMEM) medium (SH30022.01, GE Healthcare Life Sciences, Logan, UT, USA) supplemented with 10% fetal bovine serum, 4.5 g/L glucose, 4.0 mM L-glutamine, and sodium pyruvate. The cells were maintained in a humidified 5% CO_2 atmosphere at 37 °C. To induce autophagy, the cells were subjected to starvation conditions. Specifically, the day after transfection, the cells were washed three times with phosphate-buffered saline (PBS, SH30256.01B, Thermo Fisher Scientific, Waltham, MA, USA) and then starved in EBSS for 2 hours at 37 °C in a humidified CO_2 incubator. HEK293T cell lines were validated by short tandem repeat (STR) profiling and tested negative for mycoplasma.

2.3 Transfection

HEK293T cells were transfected with plasmid DNA using Lipofectamine 2000 (Thermo Fisher Scientific, Waltham, MA, USA), following the manufacturer's protocol. Briefly, HEK293T cells were seeded in confocal dishes (801001, NEST Biotechnology Co., Ltd., Wuxi, China). On the day of transfection, the cells were 50 to 60% confluent. For each dish of cells, dilute 2 µg of plasmid DNA into 150 µL of OptiMEM Medium (Gibco, Waltham, MA, USA) and mix gently. Then, dilute 4 µL of Lipofectamine 2000 into 150 µL OptiMEM Medium (Gibco, Waltham, MA, USA), mix gently and incubate for 5 min at room temperature. Add the diluted DNA to the diluted Lipofectamine 2000, mix gently and incubate for 20 minutes at room temperature. Add DNA-lipid complexes to cells. Incubate the cells at 37 °C in a CO_2 incubator. After 5 hours, the DNA-lipid complexes were removed and the fresh complete culture medium was added until ready to assay.

2.4 LysoTracker Probes Staining

Following starvation treatment, a portion of the HEK293T cells was stained with LysoTracker Deep Red (50 nM) for 30 minutes. LysoTracker probes label acidic organelles, primarily lysosomes. The cells were then washed three times with PBS (SH30256.01B, Thermo Fisher Scientific, Waltham, MA, USA), resuspended in PBS, and subjected to confocal microscopy (Leica Microsystems Inc., Mannheim, Germany) analysis.

2.5 DAPI Staining

After 24 hours of transfection and subsequent treatment, HEK293T cells were fixed with 4% paraformaldehyde (A500684-0500, Sangon Biotech Co., Ltd., Shanghai, China) in PBS for 10 minutes at room temperature. The cells were then washed three times with PBS, incubated for 5 minutes in 0.1% Triton X-100 (A600198-0500, Sangon Biotech Co., Ltd., Shanghai, China) in PBS, and washed again three times with PBS. The samples were stained with DAPI (300 nM) for five minutes and washed three more times with PBS. Finally, the samples were resuspended in PBS and subjected to confocal microscopy analysis.

2.6 Confocal Microscopy

Fluorescence images were captured using a Leica TCS SP5 confocal microscope (Leica Microsystems Inc., Mannheim, Germany) equipped with a 63× oil immersion objective. The results were obtained in sequential scan mode, with samples selectively excited at laser wavelengths of 405 nm, 488 nm or 633 nm. Images were acquired using LAS AF Lite software 2.6 (Leica Microsystems Inc., Mannheim, Germany). The scale bars in the images represent either 5 µm or 10 µm.

2.7 Statistical Analysis

Data are shown from a single experiment by confocal microscopy with technical duplicates (6 fields per dish). The data were expressed as mean ± standard deviation (SD), and each experiment was repeated at least three times. The statistical analyses were conducted by unpaired stu-

dent's *t*-test using GraphPad Prism 9.0 software (GraphPad Software Inc., San Diego, CA, USA). The differences were considered statistically significant when the *p*-value was less than 0.05.

3. Results and Discussion

3.1 The Existence of Massive Vacuole in HEK293T Cells

In general, vacuoles are considered organelles responsible for disposing of cellular waste in eukaryotic cells. According to previous reports, various factors, such as carbon tetrachloride, osmotic swelling and alterations in membrane tension, are believed to play key roles in vacuole formation [25–28].

In this study, HEK293T cells were transfected with the pEGFP-LC3B vector, and LC3B-EGFP aggregation was visualized using a confocal microscope. As shown in Fig. 1A, treatment with EBSS significantly induced autophagosome formation, as evidenced by the presence of green LC3B-EGFP puncta in HEK293T cells (arrow 1). Interestingly, intracellular massive vacuoles were also observed in HEK293T cells, which were negative for LC3B-EGFP (Fig. 1A, arrow 2). Unlike the results described above, vacuoles were not observed during fatiguing stimulation in muscle cells; however, vacuole formation has been reported during the recovery period [29]. This discrepancy may be due to differences in cell types, leading to completely opposite responses to starvation. In the adenine-induced CKD (chronic kidney disease) mice, the vacuolization of renal tubular epithelial cells was also reported [30].

By overlaying bright-field and dark-field images, it was clearly shown that these large intracellular vesicles were localized between the plasma membrane and the nucleus, with some filled with fluids and small vesicles or pellets (Fig. 1B). As showing in Fig. 1C, starvation prominently induced the formation of massive vacuoles compared with the control group cultivated in complete medium ($p < 0.05$). We observed that small vesicles could quickly enter larger vesicles (Fig. 1D, upper panel). As shown in Fig. 1D (lower panel, T: 00:00), a small, dark-colored vesicle (red arrow) and a small, light-colored vesicle (yellow arrow) were positioned near a relatively large vesicle (blue arrow). The two small vesicles then moved rapidly toward the large vesicle (Fig. 1D, T: 00:22). Subsequently, the small, light-colored vesicle made contact with the large vesicle (Fig. 1D, T: 00:55). Eventually, the small, light-colored vesicle completely entered the large vesicle (Fig. 1D, T: 01:41). Further confocal analysis suggested that the fusion of small intracellular vesicles might also lead to the formation of large vacuoles. As shown in Fig. 1E, two small vesicles have just fused, and the contour cut between the vesicles is clearly visible (arrow 1).

3.2 Heterogeneity of Massive Vacuole in HEK293T Cells

We discover that a typical feature of massive vacuoles is their heterogeneity. To verify the biological properties of massive vacuoles, HEK293T cells were transfected with an EGFP-LC3B-encoding plasmid, treated with EBSS, and stained with LysoTracker Deep Red, which labels lysosomal compartments. Some massive vacuoles were LysoTracker Deep Red-negative, indicating that these vacuoles had a non-acidic internal pH in their initial state (Fig. 2A). However, Fig. 2B highlights the presence of acidic massive vacuoles (arrow 1) that are significantly larger than primary lysosomes (arrow 2). Interestingly, some massive vacuoles exhibited heterogeneity. As illustrated in Fig. 2C, several secondary lysosomes, which were positive for LysoTracker Deep Red, were present within a massive vacuole; however, the matrix of the vacuole was negative for LysoTracker Deep Red. LysoTracker Deep Red staining also demonstrated variability in pH among different massive vacuoles. Fig. 2D shows that the pH of these vacuoles was heterogeneous. Moreover, significant differences in pH values were observed among different autolysosomes (data not shown). We also observed that lysosomes and autophagosomes could coexist within some massive vacuoles (Fig. 2E).

3.3 Formation of Acidic Massive Vacuole by Lysosome Accumulating or Fusion

In this study, we identified two mechanisms by which small lysosomes can form acidic massive vacuoles. The first mechanism involves the accumulation of small lysosomes into a large vacuole. We found that lysosomes play an important role in the formation of acidic massive vacuoles. As shown in Fig. 3A, a primary lysosome was localized around a massive vacuole in the cytoplasm. The primary lysosome then moved toward and entered the massive vacuole within 60 seconds. Interestingly, we observed that secondary lysosomes could also enter the massive vacuole directly. Fig. 3B illustrates a secondary lysosome partially entering a massive vacuole. Additionally, the fusion of small vacuoles with a massive vacuole was dynamically observed.

The second mechanism involves the fusion of small acidic vacuoles, resulting in the formation of an acidic massive vacuole. Fig. 3C shows two small vacuoles near a massive vacuole. After 220 seconds, the two small acidic vacuoles directly fused with the massive vacuole. Consistent with this, Henics T also suggested that the fusion of small intracellular vesicles might be the primary mechanism leading to the formation of massive vacuoles [31]. We found that a small, light-colored vesicle could completely enter a large vesicle in less than 2 minutes (Fig. 1D). Moreover, the fusion of small vacuoles can occur between neighboring cells (data not shown).

3.4 Formation of Lysosome-Like Massive Vacuoles

Under conditions of nutrient starvation, we observed that not only small vacuoles but also lysosomes (Fig. 4), autophagosomes (Fig. 5), and autolysosomes (Fig. 6) could

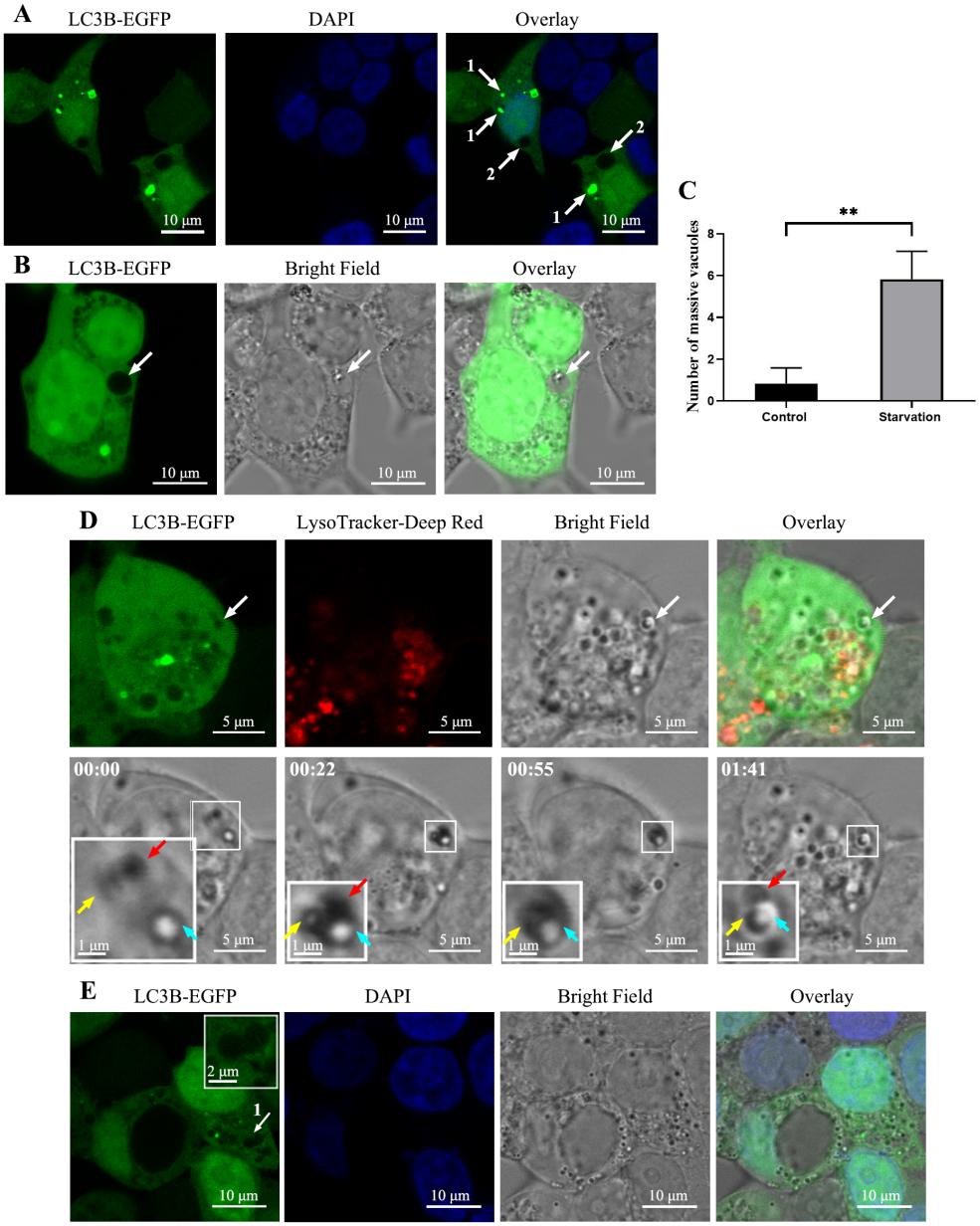

Fig. 1. Detection of massive vacuole in HEK293T cells. (A) HEK293T cells were transfected with an pEGFP-LC3B encoding plasmid and subsequently treated with EBSS for 2 hours to induce starvation. After treatment, the cells were stained with DAPI, and representative fluorescence images were captured. Scale bars: 10 μm. Arrow1: autophagosome, arrow2: LC3B-EGFP- massive vacuoles. (B) HEK293T cells were transfected with pEGFP-LC3B vectors. Following an additional 24-hour incubation, the cells were starved using EBSS and analyzed with a confocal microscope at 63× magnification. Scale bars: 10 μm. Arrow: massive vacuole. (C) HEK293T cells were transfected with the EGFP-LC3B plasmids, and then treated with EBSS or complete medium. The cells were stained with Lysotracker-Deep Red and analyzed with a confocal microscope. The quantity of massive vacuoles was compared between the starvation group and the control group. $^{**}p < 0.01$ compared with the control group cultivated in complete medium. n = 6. Red arrow: a small dark-colored vesicle, yellow arrow: a small light-colored vesicle, blue arrow: a relatively large vesicle. (D) HEK293T cells were transfected with an EGFP-LC3B encoding plasmid and subsequently treated with EBSS or complete medium. Following this treatment, the cells were stained with Lysotracker-Deep Red, and representative fluorescence images were captured. The left panels display magnified views of the boxed areas from the right panels. Red or yellow arrows indicate small vesicles, while blue arrows denote large vesicles. Scale bar1: 5 μm. Scale bar2: 1 μm (Enlarged image). (E) HEK293T cells were transfected with a pEGFP-LC3B encoding plasmid, treated with EBSS, stained with DAPI, and then analyzed using a confocal microscope at 63× magnification. Scale bar1: 10 μm. Scale bar2: 2 μm (Enlarged image). Arrow: two vesicles just fused. EGFP, enhanced green fluorescent protein; LC3B, light chain 3; DAPI, 4′, 6-diamidino-2-phenylindole; EBSS, Earle's balanced salt solution.

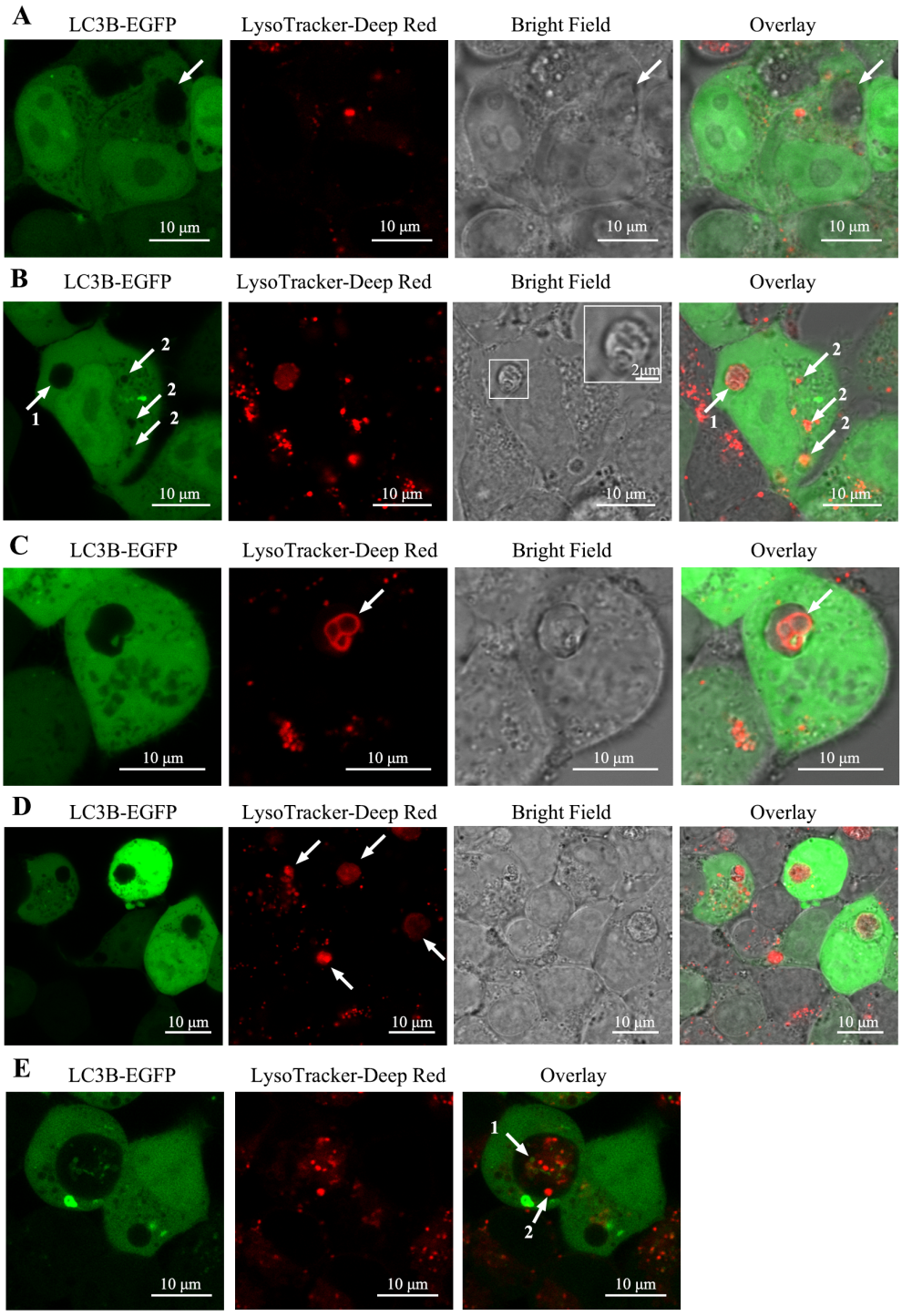

Fig. 2. Heterogeneity of massive vacuole in HEK293T cells. HEK293T cells were transfected with the pEGFP-LC3B plasmid. After treatment with EBSS, the cells were stained with LysoTracker Deep Red. The cells were then analyzed using confocal microscopy at 63× magnification. Scale bar: 10 μm. (A) Initially, the internal pH of some massive vacuoles was non-acidic. Arrow: a non-acidic massive vacuole. (B) Some massive vacuoles exhibited acidic properties and were significantly larger than primary lysosomes. Scale bar1: 10 μm. Scale bar2: 2 μm (Enlarged image). Arrow1: acidic massive vacuole, arrow2: primary lysosome. (C) Several secondary lysosomes could appear simultaneously within a massive vacuole. Arrow: secondary lysosomes. (D) The pH of massive vacuoles was significantly heterogeneous in HEK293T cells. Arrow: massive vacuoles with different acidity contents. (E) Both lysosomes and autophagosomes could coexist within a single massive vacuole. Arrow1: autophagosomes, arrow2: lysosomes.

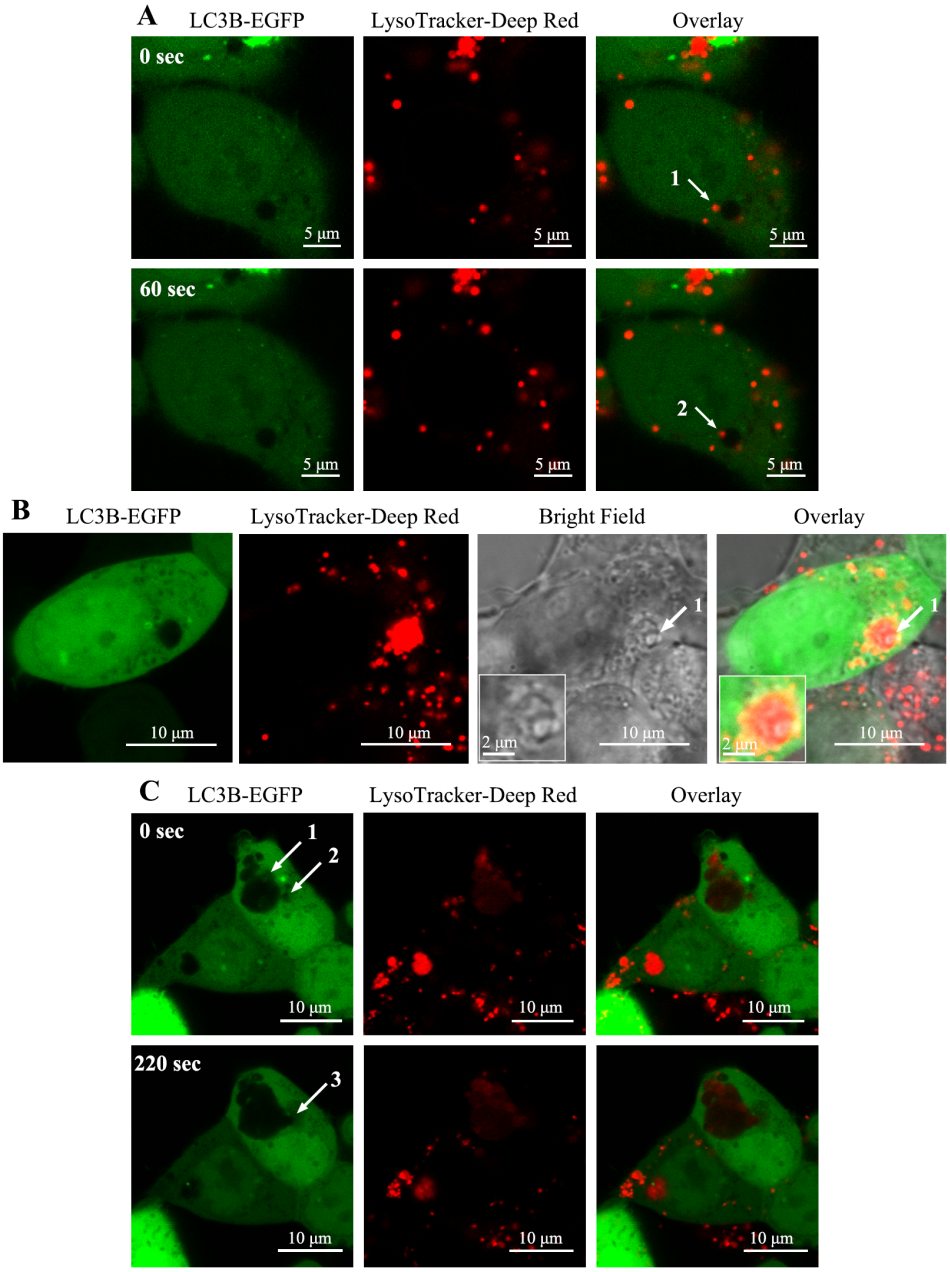

Fig. 3. Formation of acidic massive vacuole. HEK293T cells were transfected with the pEGFP-LC3B plasmid. Twenty-four hours after transfection, the cells were starved in EBSS, followed by staining with LysoTracker Deep Red. The cells were then analyzed using confocal microscopy. (A) The dynamic process of a primary lysosome entering a massive vacuole. Scale bar: 5 μm. Arrow1: a primary lysosome near a massive vacuole, arrow2: a primary lysosome just entered a massive vacuole. (B) A secondary lysosome partially entering a massive vacuole. Scale bar1: 10 μm. Scale bar2: 2 μm (Enlarged image). Arrow1: a secondary lysosome. (C) Dynamic viewing of fusion of the acidic vesicles and a massive vacuole in HEK293T cells. Scale bar: 10 μm. Arrow1, 2: small vacuoles near a massive vacuole, arrow3: massive vacuole after fusion.

form massive vacuoles with distinct characteristics. As shown in Fig. 4A, lysosome-like massive vacuoles were observed in HEK293T cells. It is noteworthy that the periphery of these lysosome-like massive vacuoles was Lysotracker Deep Red positive, while the central region was negative. Confocal images revealed that the diameter of the initial lysosome-like massive vacuoles reached 2.5 μm. Notably, some subcellular organelles were observed entering these lysosome-like vacuoles. As shown in Fig. 4B (top row), a small vesicle (Lysotracker Deep Red negative) was entering a lysosome-like massive vacuole, with half of the vesicle already inside (arrow 1). After 18 minutes, the small vesicle (Lysotracker Deep Red negative) had fully entered the lysosome-like massive vacuole (arrow 2). Moreover, a

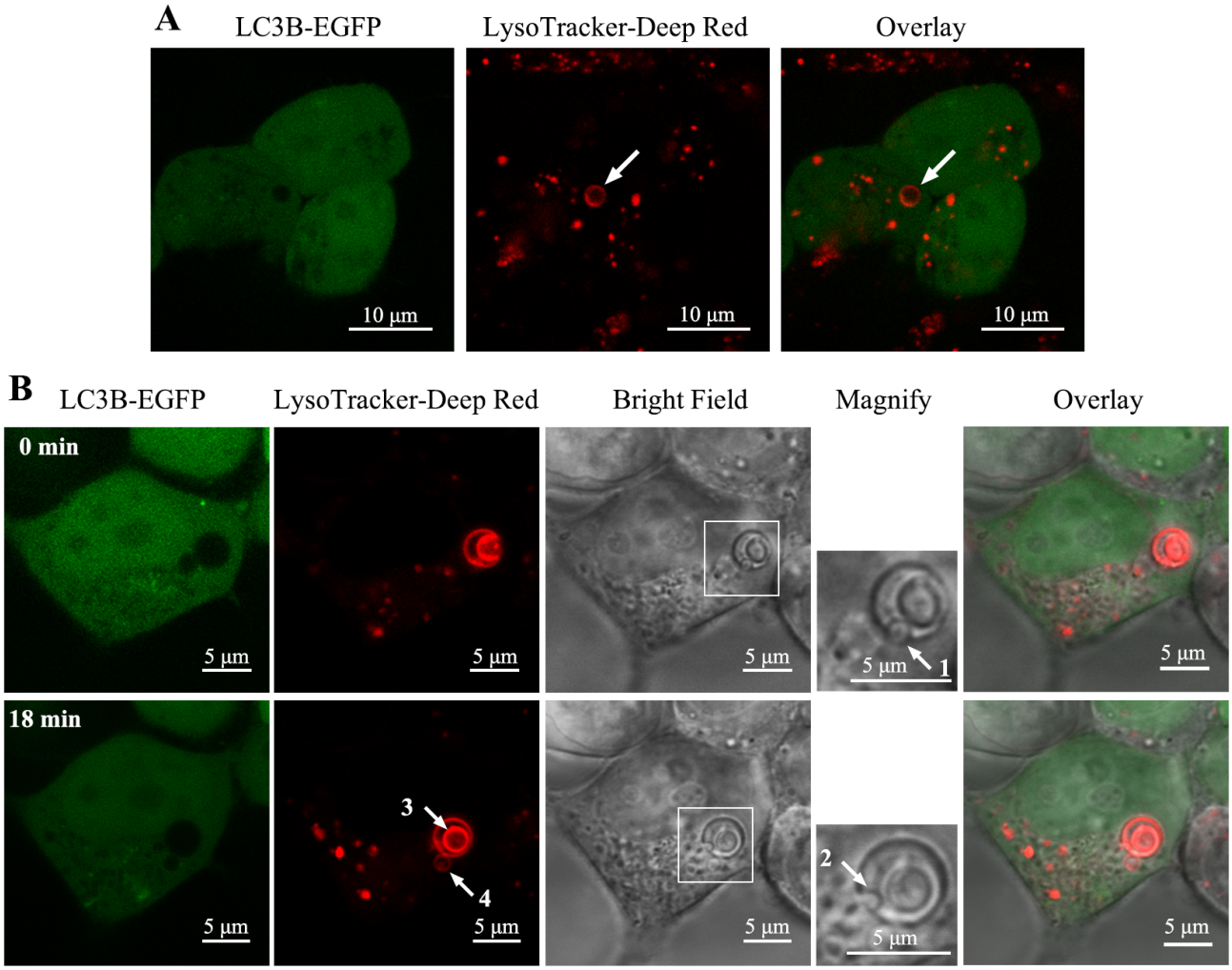

Fig. 4. Formation of massive vacuole originates from lysosome-like vacuoles. HEK293T cells were transiently transfected with the pEGFP-LC3B plasmid and cultured for 24 hours. The cells were then starved in EBSS. After staining with LysoTracker Deep Red, fluorescent signals were examined using confocal microscopy. Representative fluorescence images are shown. (A) The presence of lysosome-like massive vacuole in HEK293T cells transfected with the pEGFP-LC3B plasmid. Scale bars: 10 μm. Arrow: lysosome-like massive vacuole. (B) Dynamic observation of small vesicles entering lysosome-like massive vacuole. Scale bars: 5 μm. Arrow1: a small vesicle (Lysotracker Deep Red negative) entering a lysosome-like massive vacuole, arrow2: a small vesicle (Lysotracker Deep Red negative) just entered a lysosome-like massive vacuole, arrow3: small vacuole (Lysotracker Deep Red positive) in a lysosome-like massive vacuole, arrow4: small vacuole (Lysotracker Deep Red positive) near a lysosome-like massive vacuole.

small vacuole (Lysotracker Deep Red positive) was already present within the lysosome-like massive vacuole (arrow 3), while another small vacuole (Lysotracker Deep Red positive) was adjacent to it and about to enter (arrow 4).

3.5 Formation of Autophagosome-Like Massive Vacuole

In HEK293T cells transfected with the pEGFP-LC3B vector, autophagosomes of varying sizes were readily observed (Fig. 5A, arrows 1 and 2). Additionally, autophagosome-like vacuoles were present in the cytoplasm (Fig. 5A, arrow 3). As shown in Fig. 5B1, a small autophagosome was initially located on the membrane of an autophagosome-like massive vacuole; shortly thereafter, the small autophagosome entered it (Fig. 5B2). Interestingly, we found a small autophagosome-like vacuole can directly enter an autophagosome-like massive vacuole. Fig. 5C1 showed a small autophagosome-like vacuole was passing through the membrane of an autophagosome-like massive vacuole, and Fig. 5C2 showed another small autophagosome-like vacuole had entered an autophagosome-like massive vacuole (Fig. 5C2).

3.6 Formation of Autolysosome-Like Massive Vacuoles

Fig. 6A shows that LC3B-EGFP translocated to the surface membrane of the autophagosome. We observed that multiple lysosomes could accumulate within

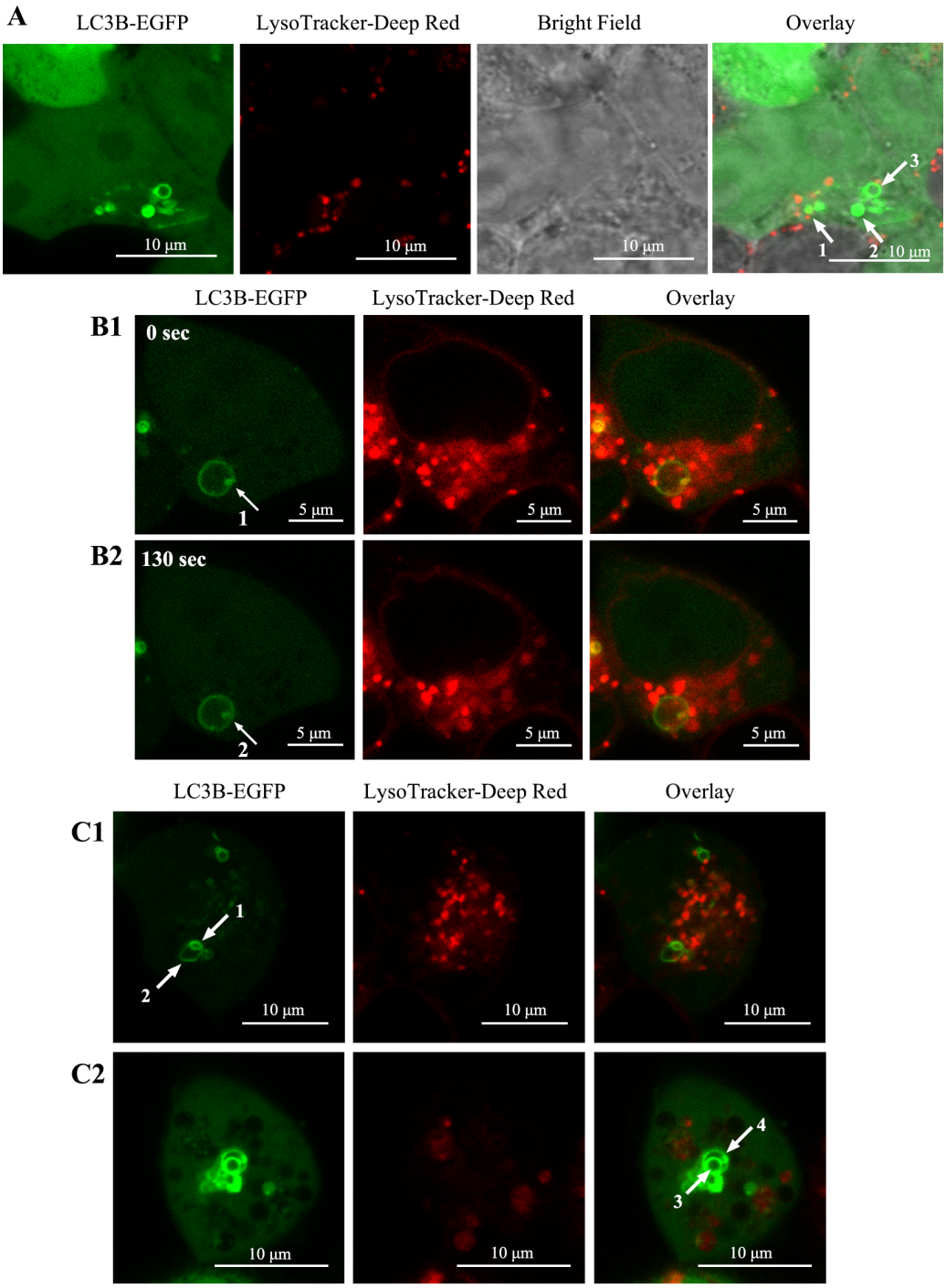

Fig. 5. Accumulation and fusion of autophagosome led to the formation of autophagosome-like massive vacuole. HEK293T cells were transfected with the pEGFP-LC3B plasmid. Twenty-four hours after transfection, the cells were starved in EBSS, followed by staining with LysoTracker Deep Red (A–C). (A) Autophagosome-like vacuoles were present in the cytoplasm of HEK293T cells transfected with the pEGFP-LC3B plasmid. Scale bars: 10 μm. Arrow1, 2: autophagosome, arrow3: autophagosome-like massive vacuole. (B1,B2) Dynamic observation of autophagosome entering autophagosome-like massive vacuole. Scale bars: 5 μm. Arrow1: autophagosome located on the membrane of an autophagosome-like massive vacuole. arrow2: autophagosome just entered an autophagosome-like massive vacuole. (C1,C2) Autophagosome-like vacuoles could merge into autophagosome-like massive vacuole. Scale bars: 10 μm. Arrow1: a small autophagosome-like vacuole passing through the membrane of an autophagosome-like massive vacuole, arrow2: an autophagosome-like massive vacuole, arrow3: a small autophagosome-like vacuole, arrow4: an autophagosome-like massive vacuole.

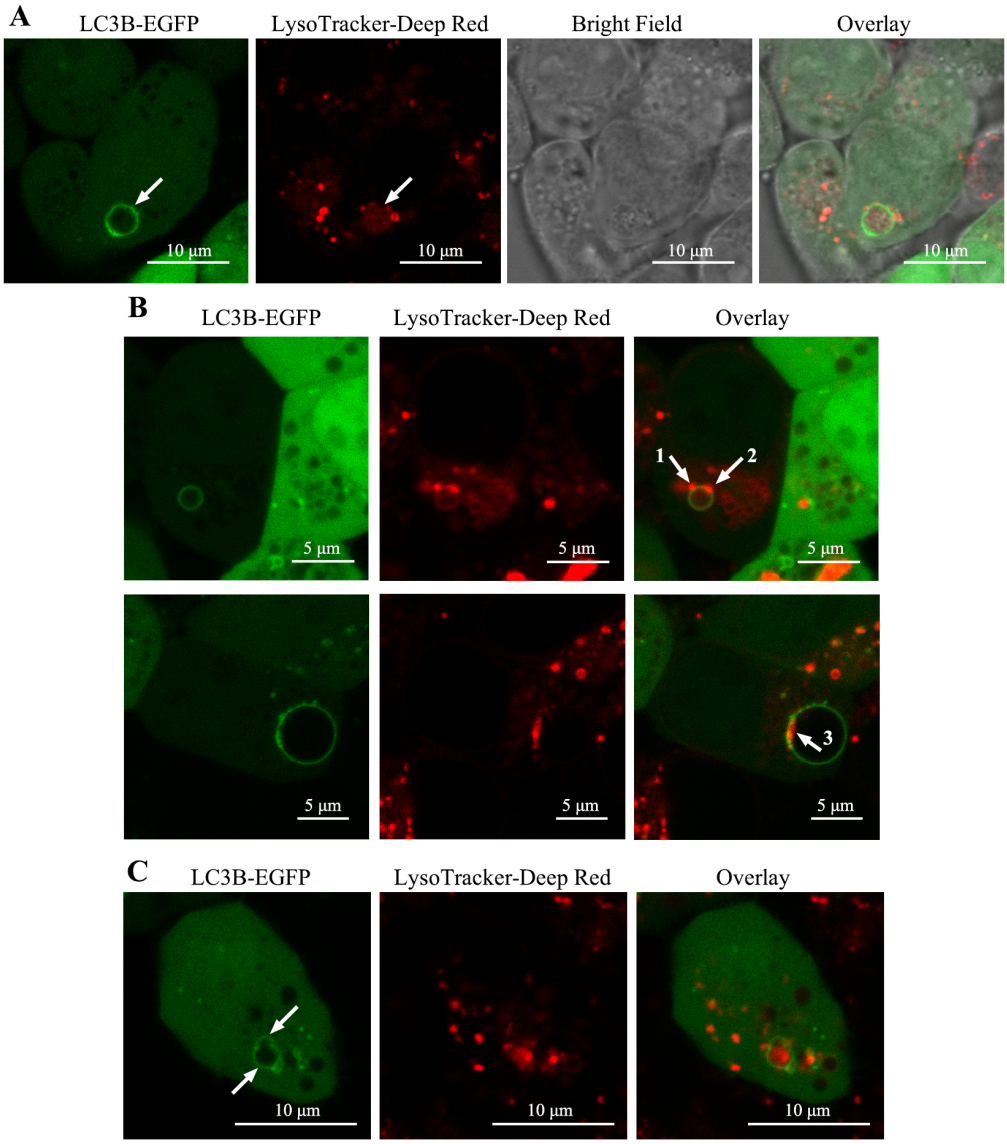

Fig. 6. Formation of autolysosome-like massive vacuoles. HEK293T cells were transiently transfected with the pEGFP-LC3B plasmid and then incubated in EBSS medium to induce starvation. Subsequently, the cells were stained with LysoTracker Deep Red, and analyzed using confocal microscopy. (A) The presence of autolysosome-like massive vacuoles in HEK293T cells transfected with the pEGFP-LC3B plasmid. Scale bars: 10 μm. Arrow: an autolysosome-like massive vacuole. (B) The accumulation of lysosomes leads to the formation of autolysosome-like massive vacuoles. Scale bars: 5 μm. Arrow1: a lysosome in contact with an autolysosome-like massive vacuole, arrow2: a lysosome localized on the membrane of an autolysosome-like massive vacuole, arrow3: lysosomes inside an autolysosome-like massive vacuole. (C) Fusion of autolysosomes results in the formation of autolysosome-like massive vacuoles. Scale bars: 10 μm. Arrow: autolysosome-like vacuoles just fused.

the autophagosome, leading to the formation of large autolysosome-like vacuoles. As shown in Fig. 6B (top row), one lysosome was in contact with an autophagosome (indicated by arrow 1), while another lysosome was localized on the membrane of the autophagosome (indicated by arrow 2). Upon entering the autophagosome, some lysosomes may remain close to its inner membrane for a short period (Fig. 6B, bottom row).

Furthermore, the fusion of autolysosomes can also contribute to the formation of autolysosome-like massive vacuoles. Fig. 6C illustrates that two autolysosome-like vacuoles have just fused, and their external contours still maintain their original shape (indicated by arrowheads), with significant differences in their contents.

3.7 Autolysosomes have Strong Mobility

Using laser confocal microscopy, we observed that some autolysosomes were highly mobile, with the distance between them continuously changing. At the moment of initiation, the distance between two autolysosomes

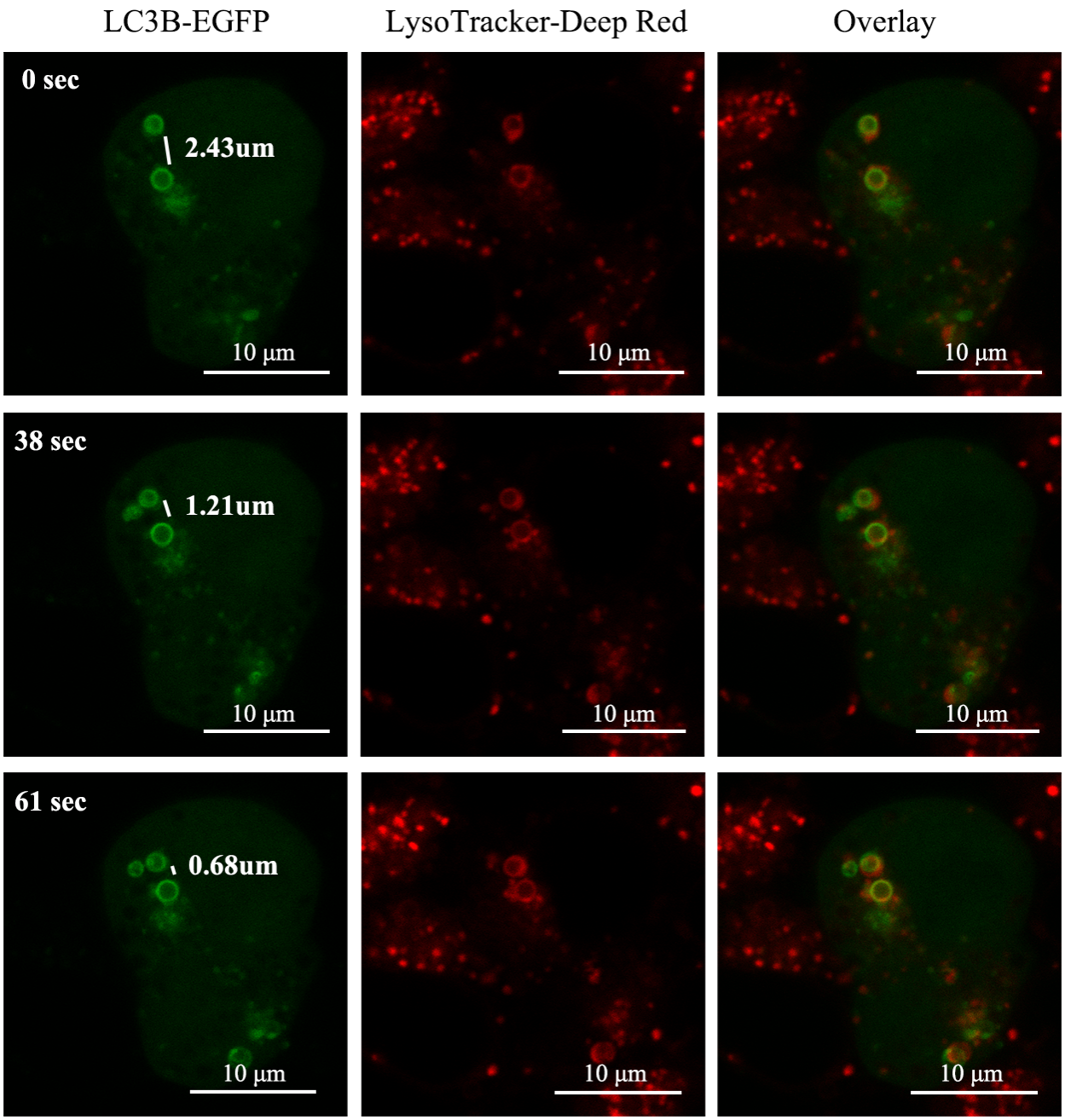

Fig. 7. Analysis of the motility of autolysosomes. HEK293T cells were transiently transfected with the pEGFP-LC3B plasmid and then incubated in EBSS medium to induce starvation. Subsequently, the cells were stained with LysoTracker Deep Red, and analyzed using confocal microscopy. Scale bar: 10 μm.

was 2.43 μm (Fig. 7, 0 sec). After 38 seconds, this distance decreased to 1.21 μm, and after 61 seconds, it further decreased to 0.68 μm. These results suggest that high-speed mobility may increase the likelihood of autolysosomes coming into contact with each other, potentially leading to the formation of autolysosome-like massive vacuoles.

These findings suggest that the high mobility of autolysosomes may increase the likelihood of contact between different organelles, potentially leading to the formation of massive autolysosome vacuoles. Other subcellular organelles with high mobility, such as mitochondria, have also been reported to be essential for maintaining mitochondrial functional homeostasis [32].

3.8 Bi-Layer Membrane Structure of Massive Vacuole

Additionally, we discovered that lysosome-like massive vacuoles or autolysosome-like massive vacuoles could exist in a double-membrane structure (Fig. 8). Wolff *et al.* [33] reported that coronaviruses can induce the for-

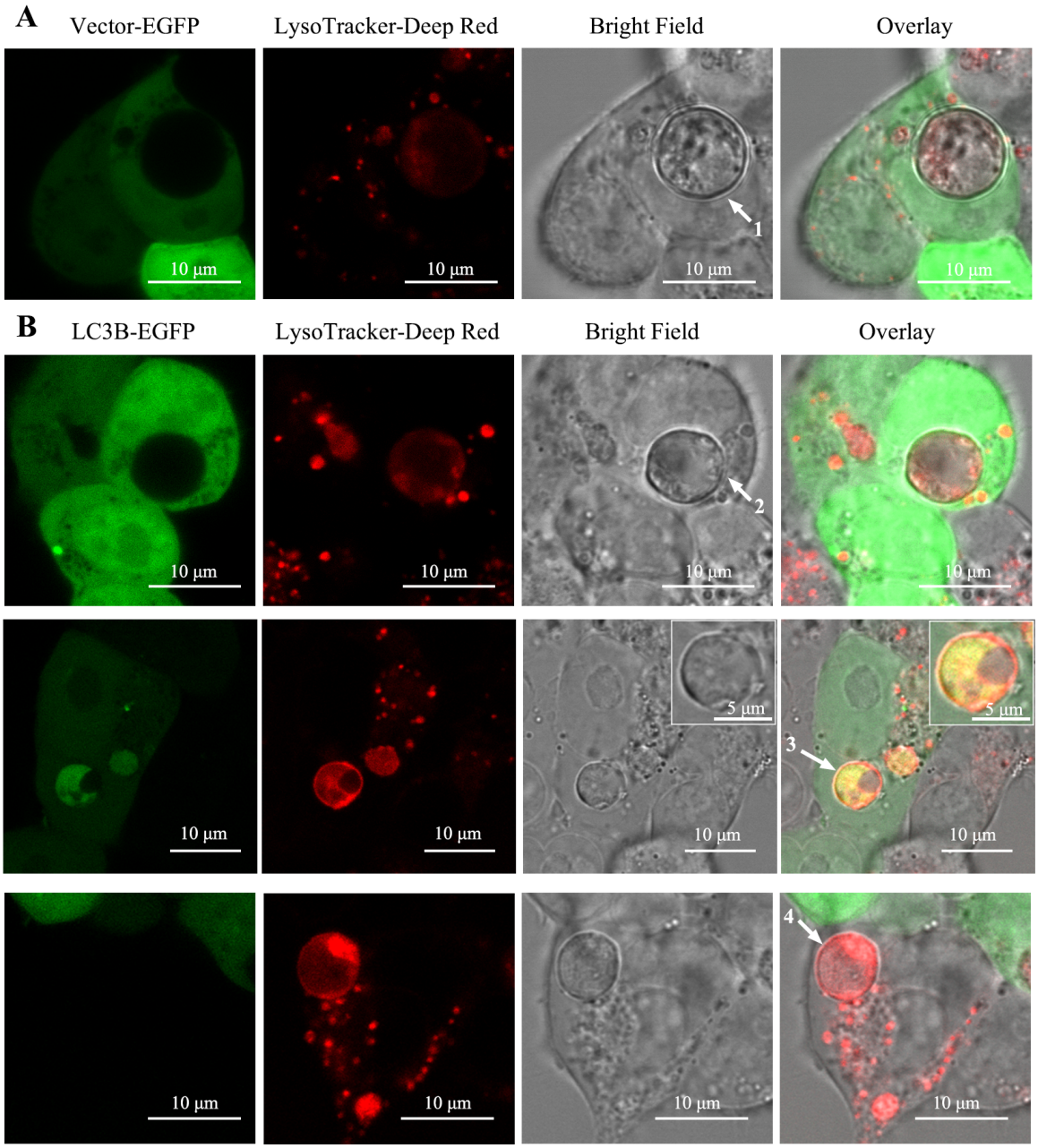

Fig. 8. Several types of massive vacuoles possessed double-layer membrane structure. HEK293T cells were transiently transfected with either the pEGFP-N3 plasmid (A) or pEGFP-LC3B plasmid (B) and cultured for 24 hours. The cells were then incubated in EBSS medium, followed by staining with LysoTracker Deep Red and analyzed using confocal microscopy. (A) Lysosome-like massive vacuoles with a bilayer membrane structure were observed in HEK293T cells. Scale bars: 10 μm. Arrow1: a bilayer membrane structure. (B, top row) Lysosome-like massive vacuoles with a bilayer membrane structure were observed in HEK293T cells. Scale bars: 10 μm. Arrow2: a bilayer membrane structure of lysosome-like massive vacuoles. (B, middle row) Autolysosome-like massive vacuoles with a bilayer membrane structure were present in HEK293T cells. Scale bar1: 10 μm. Scale bar2: 5 μm (Enlarged image). Arrow3: a bilayer membrane structure of autolysosome-like massive vacuoles. (B, bottom row) Lysosome-like massive vacuoles with a double membrane were found in LC3B-EGFP-negative HEK293T cells. Scale bars: 10 μm. Arrow4: a bilayer membrane structure.

mation of cytosolic double-membrane vesicles in infected cells, which may provide a suitable microenvironment for viral RNA synthesis. Doyle *et al.* [34] also suggested that all coronavirus genera can induce the formation of double-membrane vesicles. Moreover, Pérez-Cruz *et al.* [35] discovered that outer-inner membrane vesicles can be detected in Gram-negative pathogenic bacteria, which deliver cytoplasmic components into the vesicles.

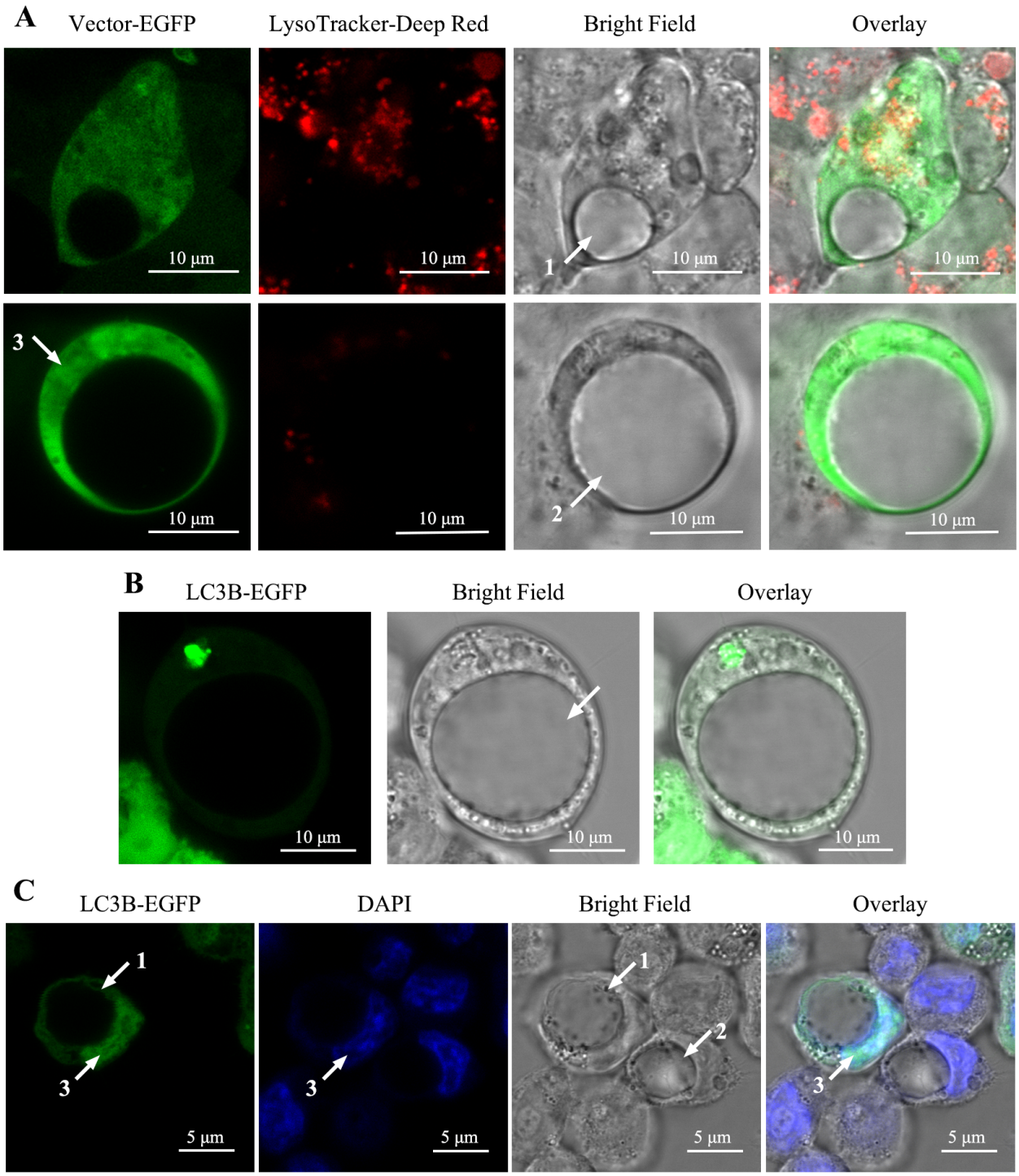

Fig. 9. HEK293T cell with massive vacuole could form signet ring like cells. (A) HEK293T cells were transfected with the pEGFP-N3 plasmid, then incubated in EBSS medium, followed by incubation with LysoTracker Deep Red. Confocal microscopy was used to detect the presence of signet ring-like cells. Scale bar: 10 μm. Arrow1: massive vacuole, arrow2: enlarged massive vacuole, arrow3: cellular content (the cytoplasm and nucleus). (B) Signet ring-like cells were also observed in HEK293T cells transfected with the pEGFP-LC3B plasmid, treated with EBSS. Scale bars: 10 μm. (C) The nuclear morphology of signet ring-like cells derived from HEK293T cells was assessed. HEK293T cells were transfected with the pEGFP-LC3B plasmid, treated with EBSS and stained with DAPI. Scale bars: 5 μm. Arrow1: massive vacuole in LC3B-positive HEK293T cells, arrow2: massive vacuole in LC3B-negative HEK293T cells, arrow3: the nucleus ($DAPI^+$).

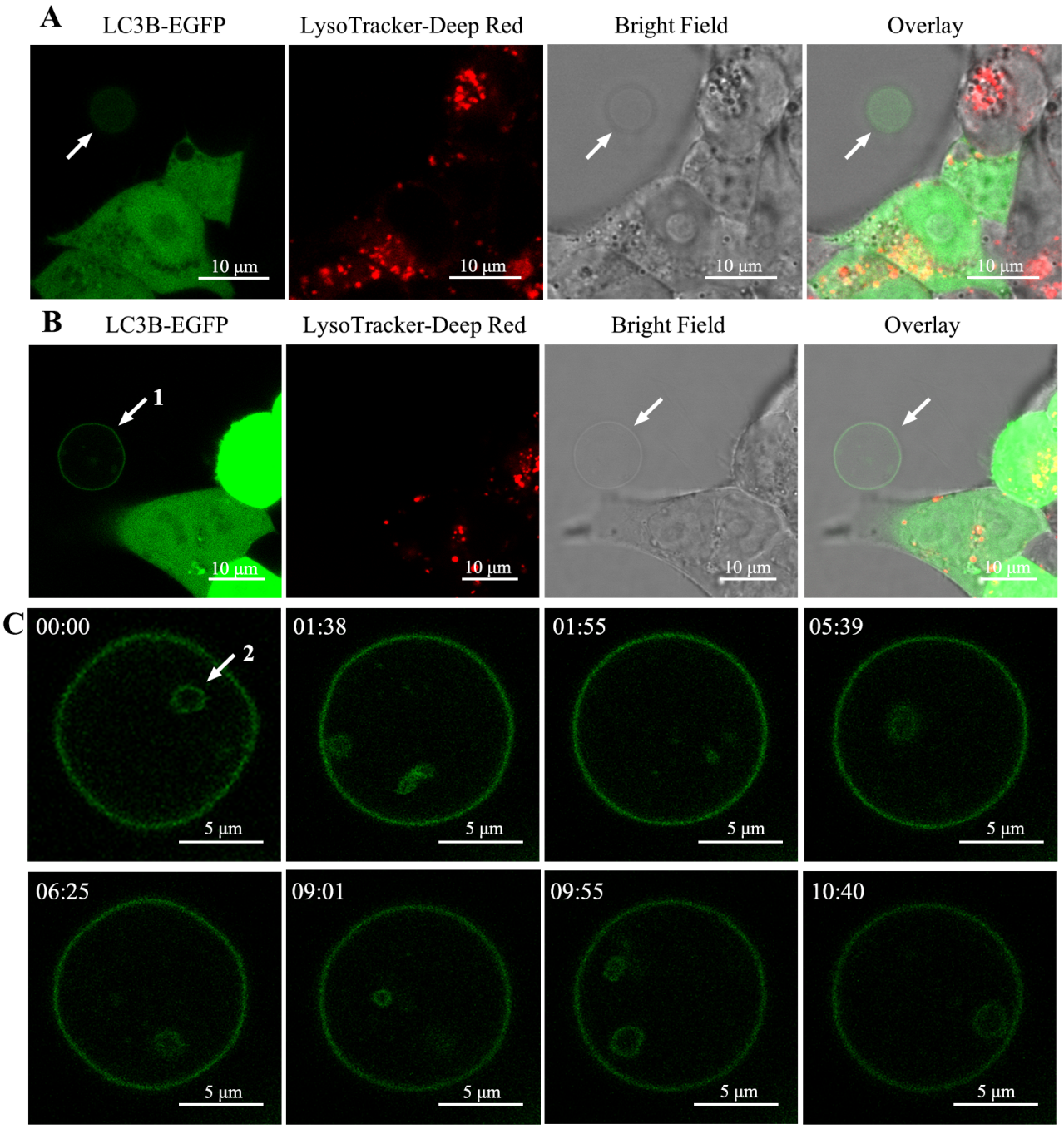

Fig. 10. Dynamic movement of autophagosome-like structures in extracellular autophagosome-like massive vacuole. HEK293T cells were transfected with the pEGFP-LC3B plasmid, then incubated in EBSS medium (starvation), followed by staining with LysoTracker Deep Red. (A) The presence of an LC3B-EGFP-positive massive vacuole outside HEK293T cells. Scale bars: 10 μm. Arrow: a massive vacuole filled with LC3B-EGFP fluorescent proteins. (B) The presence of an autophagosome-like massive vacuole outside HEK293T cells. Scale bars: 10 μm. Arrow1: an autophagosomelike massive vacuole outside HEK293T cells. (C) High-speed mobility of autophagosome-like structures within the autophagosome-like massive vacuole. Scale bars: 5 μm. Arrow2: autophagosome-like structures within the autophagosome-like massive vacuole.

When HEK293T cells were transfected with the pEGFP-N3 plasmid, confocal laser microscopy revealed the presence of lysosome-like massive vacuole (indicated by arrows) in the cytoplasm. The vacuole was filled with several eosinophilic materials and its membranes exhibited a bilayer structure (Fig. 8A). To further assess the membrane characteristics of these vacuoles, HEK293T cells were transfected with pEGFP-LC3B. As shown in Fig. 8B

(top row), a lysosome-like massive vacuole, which was LC3B-negative and Lysotracker DeepRed-positive, was present in the cytoplasm with a double membrane. Moreover, an autolysosome-like massive vacuole, which was both LC3B-positive and Lysotracker-positive, was also observed in the cytoplasm with a double membrane (Fig. 8B, middle row). In LC3B-EGFP-negative HEK293T cells, confocal analysis revealed that a lysosome-like massive vacuole with a double membrane could be found in the cytoplasm (Fig. 8B, bottom row). In summary, large lysosome-like or autolysosome-like massive vacuoles can exist with a double membrane structure.

3.9 Formation of Signet Ring like Cell in HEK293T Cells

In pEGFP-transfected HEK293T cells, EGFP fluorescence proteins were distributed in both the cytosol and nucleus (Fig. 9A, top row). Under starvation conditions, we observed a massive vacuole that was negative for both EGFP and Lysotracker DeepRed. The massive vacuole appeared semi-transparent under bright-field microscopy. Moreover, the volume of the massive vacuole gradually increased, causing the cytoplasm and nucleus to be compressed to the periphery of the HEK293T cells (Fig. 9A, bottom row).

Massive vacuoles were also observed in HEK293T cells transfected with the pLC3B-EGFP plasmid (Fig. 9B, arrow). These vacuoles occupied the majority of the intracellular space. LC3B-EGFP puncta were rarely observed in the large vacuole but were present in the cytoplasm. As a result, HEK293T cells containing massive vacuoles resembled signet ring-like cells. As shown in Fig. 9C, the nucleus was pushed to the edge (indicated by arrow 3), and the cytoplasmic region outside the vacuole was minimal. Many epithelial tumors contain large amounts of mucin glycoproteins, leading to the formation of cytoplasmic vacuoles and the displacement of the nucleus to the cell periphery, creating a signet-ring-like structure [36,37]. In pathology, signet ring cells are often associated with adenocarcinomas and show significant heterogeneity [38,39]. Song IH *et al.* [40] reported that mucinous adenocarcinoma with a signet ring cell component was commonly associated with poor overall survival and recurrence-free survival.

Interestingly, massive vacuoles, which contained fewer vesicles and appeared transparent, were also found in LC3B-negative HEK293T cells (indicated by arrow 2 in Fig. 9C). These results indicate that there is no significant relationship between LC3B and the formation of signet ring-like cells. In the microenvironment of excessive growth of tumor cells, nutrient deficiency may be an important factor in the production of signet ring cells.

3.10 Autophagosome-Like Massive Vacuole Outside HEK293T Cells

Occasionally, a massive vacuole filled with LC3B-EGFP fluorescent proteins was observed outside HEK293T cells transfected with the LC3B-EGFP plasmid (Fig. 10A, indicated by the arrow). Moreover, an autophagosome-like massive vacuole was detected outside HEK293T cells expressing LC3B-EGFP (Fig. 10B, indicated by the arrow), with LC3B-EGFP stably localized on its membrane. Furthermore, several autophagosome-like structures were present within the autophagosome-like massive vacuole, exhibiting rapid and undirected movement (Fig. 10C). The reconstructed dynamic images of the autophagosome-like structures were showed in the **Supplementary Data**. These findings suggest that further investigation into the function of the heterogeneous vacuoles outside HEK293T cells could be of significant interest.

4. Conclusions

In summary, our data indicate that nutrient deprivation induces the formation of heterogeneous, massive vacuoles in human embryonic kidney cells, some of which contribute to the development of signet ring cells, while others lead to extracellular vacuole formation.

Abbreviations

HEK, human embryonic kidney cells; LC3, Microtubule associated protein light chain 3 (MAPLC3); EGFP, Enhanced Green Fluorescent Protein; HPV, human papillomavirus; AP, Acute pancreatitis.

Availability of Data and Materials

The datasets used and/or analyzed in the current study are available from the corresponding author on reasonable request.

Author Contributions

DKS conceived, designed, and performed the experiments, and wrote the original draft. XYA and YLC performed the experiments, analyzed and interpreted the data. All authors have participated sufficiently in the work to take public responsibility for appropriate portions of the content and agreed to be accountable for all aspects of the work in ensuring that questions related to its accuracy or integrity. All authors read and approved the final manuscript. All authors contributed to editorial changes in the manuscript.

Ethics Approval and Consent to Participate

Not applicable.

Acknowledgment

Not applicable.

Funding

This study was supported by Projects of medical and health technology development program in Shandong province (grant numbers 2018WSB30002).

Conflict of Interest

The authors declare no conflict of interest.

Supplementary Material

Supplementary material associated with this article can be found, in the online version, at https://doi.org/10.31083/FBL26796.

References

[1] Aki T, Nara A, Uemura K. Cytoplasmic vacuolization during exposure to drugs and other substances. Cell Biology and Toxicology. 2012; 28: 125–131. https://doi.org/10.1007/s10565-012-9212-3.

[2] Lacombe V, Hadjadj J, Georgin-Lavialle S, Lavigne C, Geneviève F, Kosmider O. Vacuoles in bone marrow progenitors: VEXAS syndrome and beyond. The Lancet. Haematology. 2024; 11: e160–e167. https://doi.org/10.1016/S2352-3026(23)00375-7.

[3] Shubin AV, Demidyuk IV, Komissarov AA, Rafieva LM, Kostrov SV. Cytoplasmic vacuolization in cell death and survival. Oncotarget. 2016; 7: 55863–55889. https://doi.org/10.18632/oncotarget.10150.

[4] Ikonomov OC, Altankov G, Sbrissa D, Shisheva A. PIKfyve inhibitor cytotoxicity requires AKT suppression and excessive cytoplasmic vacuolation. Toxicology and Applied Pharmacology. 2018; 356: 151–158. https://doi.org/10.1016/j.taap.2018.08.001.

[5] Ritter M, Bresgen N, Kerschbaum HH. From Pinocytosis to Methuosis-Fluid Consumption as a Risk Factor for Cell Death. Frontiers in Cell and Developmental Biology. 2021; 9: 651982. https://doi.org/10.3389/fcell.2021.651982.

[6] Bielsa N, Casasampere M, Abad JL, Enrich C, Delgado A, Fabriàs G, *et al*. Methuosis Contributes to Jaspine-B-Induced Cell Death. International Journal of Molecular Sciences. 2022; 23: 7257. https://doi.org/10.3390/ijms23137257.

[7] Rajasekharan SK, Ravichandran V, Boya BR, Jayachandran A, Lee J. Repurposing methuosis-inducing anticancer drugs for anthelmintic therapy. PLoS Pathogens. 2024; 20: e1012475. https://doi.org/10.1371/journal.ppat.1012475.

[8] Schoeman R, Beukes N, Frost C. Cannabinoid Combination Induces Cytoplasmic Vacuolation in MCF-7 Breast Cancer Cells. Molecules (Basel, Switzerland). 2020; 25: 4682. https://doi.org/10.3390/molecules25204682.

[9] Chatterjee R, Setty SRG, Chakravortty D. SNAREs: a double-edged sword for intravacuolar bacterial pathogens within host cells. Trends in Microbiology. 2024; 32: 477–493. https://doi.org/10.1016/j.tim.2023.11.002.

[10] Quereda JJ, Morel C, Lopez-Montero N, Ziveri J, Rolland S, Grenier T, *et al*. A Role for Taok2 in Listeria monocytogenes Vacuolar Escape. The Journal of Infectious Diseases. 2022; 225: 1005–1010. https://doi.org/10.1093/infdis/jiaa367.

[11] Satria RD, Huang TW, Jhan MK, Shen TJ, Tseng PC, Wang YT, *et al*. Increased TNF-α Initiates Cytoplasmic Vacuolization in Whole Blood Coculture with Dengue Virus. Journal of Immunology Research. 2021; 2021: 6654617. https://doi.org/10.1155/2021/6654617.

[12] Zheng Y, Zhu G, Yan J, Tang Y, Han S, Yin J, *et al*. The Late Domain of Prototype Foamy Virus Gag Facilitates Autophagic Clearance of Stress Granules by Promoting Amphisome Formation. Journal of Virology. 2020; 94: e01719–19. https://doi.org/10.1128/JVI.01719-19.

[13] Monel B, Compton AA, Bruel T, Amraoui S, Burlaud-Gaillard J, Roy N, *et al*. Zika virus induces massive cytoplasmic vacuolization and paraptosis-like death in infected cells. The EMBO Journal. 2017; 36: 1653–1668. https://doi.org/10.15252/embj.201695597.

[14] Cai Y, Yang F, Huang X. Oxidative stress and acute pancreatitis (Review). Biomedical Reports. 2024; 21: 124. https://doi.org/10.3892/br.2024.1812.

[15] Morissette G, Moreau E, C-Gaudreault R, Marceau F. Massive cell vacuolization induced by organic amines such as procainamide. The Journal of Pharmacology and Experimental Therapeutics. 2004; 310: 395–406. https://doi.org/10.1124/jpet.104.066084.

[16] Luo Y, Guan B, Deng X, Bai P, Huang H, Miao C, *et al*. Methuosis Inducer SGI-1027 Cooperates with Everolimus to Promote Apoptosis and Pyroptosis by Triggering Lysosomal Membrane Permeability in Renal Cancer. Advanced Science (Weinheim, Baden-Wurttemberg, Germany). 2024; 11: e2404693. https://doi.org/10.1002/advs.202404693.

[17] Mahmoud MM, El-Batran SA, Hegazy R, El-Sayed WM. Taurine and enzymatically modified isoquercitrin protected against methotrexate-induced deteriorations in the conductivity and rhythmicity of the heart in rats: Antioxidant, anti-inflammatory, and histological architecture approach. Journal of Applied Toxicology: JAT. 2024; 44: 1924–1935. https://doi.org/10.1002/jat.4682.

[18] Adiguzel C, Karaboduk H, Uzunhisarcikli M. Protective Role of Melatonin Against Abamectin-Induced Biochemical, Immunohistochemical, and Ultrastructural Alterations in the Testicular Tissues of Rats. Microscopy and Microanalysis: the Official Journal of Microscopy Society of America, Microbeam Analysis Society, Microscopical Society of Canada. 2024; 30: 962–977. https://doi.org/10.1093/mam/ozae080.

[19] Reaves BJ, Bright NA, Mullock BM, Luzio JP. The effect of wortmannin on the localisation of lysosomal type I integral membrane glycoproteins suggests a role for phosphoinositide 3-kinase activity in regulating membrane traffic late in the endocytic pathway. Journal of Cell Science. 1996; 109 (Pt 4): 749–762. https://doi.org/10.1242/jcs.109.4.749.

[20] Chen R, Duan CY, Chen SK, Zhang CY, He T, Li H, *et al*. The suppressive role of p38 MAPK in cellular vacuole formation. Journal of Cellular Biochemistry. 2013; 114: 1789–1799. https://doi.org/10.1002/jcb.24522.

[21] Kroemer G, Levine B. Autophagic cell death: the story of a misnomer. Nature Reviews. Molecular Cell Biology. 2008; 9: 1004–1010. https://doi.org/10.1038/nrm2529.

[22] Kim J, Klionsky DJ. Autophagy, cytoplasm-to-vacuole targeting pathway, and pexophagy in yeast and mammalian cells. Annual Review of Biochemistry. 2000; 69: 303–342. https://doi.org/10.1146/annurev.biochem.69.1.303.

[23] Claude-Taupin A, Jia J, Mudd M, Deretic V. Autophagy's secret life: secretion instead of degradation. Essays in Biochemistry. 2017; 61: 637–647. https://doi.org/10.1042/EBC20170024.

[24] Klionsky DJ, Eskelinen EL. The vacuole versus the lysosome: when size matters. Autophagy. 2014; 10: 185–187. https://doi.org/10.4161/auto.27367.

[25] Zhou C, Vink R, Byard RW. Hyperosmolarity Induces Armanni-Ebstein-like Renal Tubular Epithelial Swelling and Cytoplasmic Vacuolization. Journal of Forensic Sciences. 2017; 62: 229–232. https://doi.org/10.1111/1556-4029.13235.

[26] Sosunov AA, McKhann Ii G, Tang G, Goldman JE. Cytoplasmic vacuolization and ectopic formation of perineuronal nets are characteristic pathologies of cytomegalic neurons in tuberous sclerosis. Journal of Neuropathology and Experimental Neurology. 2024; 83: 1047–1059. https://doi.org/10.1093/jnen/nlae079.

[27] Velle KB, Garner RM, Beckford TK, Weeda M, Liu C, Kennard AS, *et al*. A conserved pressure-driven mechanism for regulat-

ing cytosolic osmolarity. Current Biology: CB. 2023; 33: 3325–3337.e5. https://doi.org/10.1016/j.cub.2023.06.061.

[28] Yufa M, Dongmei C, Wei L, Shuangxing L, Li S, Xingchao G. Peripheral serum iTRAQ-based proteomic characteristics of carbon tetrachloride-induced acute liver injury in *Macaca fascicularis*. Toxicology Reports. 2024; 13: 101689. https://doi.org/10.1016/j.toxrep.2024.101689.

[29] Lännergren J, Bruton JD, Westerblad H. Vacuole formation in fatigued single muscle fibres from frog and mouse. Journal of Muscle Research and Cell Motility. 1999; 20: 19–32. https://doi.org/10.1023/a:1005412216794.

[30] Zhang Q, Qin Z, Wang Q, Lu L, Wang J, Lu M, *et al*. Pharmacokinetic profiling of ZCL-278, a cdc42 inhibitor, and its effectiveness against chronic kidney disease. Biomedicine & Pharmacotherapy = Biomedecine & Pharmacotherapie. 2024; 179: 117329. https://doi.org/10.1016/j.biopha.2024.117329.

[31] Henics T, Wheatley DN. Cytoplasmic vacuolation, adaptation and cell death: a view on new perspectives and features. Biology of the Cell. 1999; 91: 485–498. https://doi.org/10.1016/s0248-4900(00)88205-2.

[32] Dalmasso G, Marin Zapata PA, Brady NR, Hamacher-Brady A. Agent-Based Modeling of Mitochondria Links Sub-Cellular Dynamics to Cellular Homeostasis and Heterogeneity. PloS One. 2017; 12: e0168198. https://doi.org/10.1371/journal.pone.0168198.

[33] Wolff G, Limpens RWAL, Zevenhoven-Dobbe JC, Laugks U, Zheng S, de Jong AWM, *et al*. A molecular pore spans the double membrane of the coronavirus replication organelle. Science (New York, N.Y.). 2020; 369: 1395–1398. https://doi.org/10.1126/science.abd3629.

[34] Doyle N, Hawes PC, Simpson J, Adams LH, Maier HJ. The Porcine Deltacoronavirus Replication Organelle Comprises Double-Membrane Vesicles and Zippered Endoplasmic Reticulum with Double-Membrane Spherules. Viruses. 2019; 11: 1030. https://doi.org/10.3390/v11111030.

[35] Pérez-Cruz C, Delgado L, López-Iglesias C, Mercade E. Outer-inner membrane vesicles naturally secreted by gram-negative pathogenic bacteria. PloS One. 2015; 10: e0116896. https://doi.org/10.1371/journal.pone.0116896.

[36] Olgun A. Selective targeting of signet ring cell adenocarcinomas. Medical Hypotheses. 2019; 133: 109380. https://doi.org/10.1016/j.mehy.2019.109380.

[37] Sakalauskaite M, Garnelyte A, Civilka I, Dulskas A, Kincius M, Patasius A. Prostate Adenocarcinoma with Signet-Ring Cells and Features of Mucin: A Clinical Case and Literature Review. Medicina (Kaunas, Lithuania). 2024; 60: 877. https://doi.org/10.3390/medicina60060877.

[38] Zheng J, Liu J, Yang W, Yao J, Guo J, Liu C. The clinicopathological and immunohistochemical features of breast carcinomas with signet-ring-cell differentiation. World Journal of Surgical Oncology. 2023; 21: 181. https://doi.org/10.1186/s12957-023-03074-x.

[39] Wang Y, Li Y, Wang B, Ran D, Zhu C, Li P, *et al*. Early onset, development and histological features of gastric signet-ring cell carcinoma. Frontiers in Oncology. 2023; 13: 1166549. https://doi.org/10.3389/fonc.2023.1166549.

[40] Song IH, Hong SM, Yu E, Yoon YS, Park IJ, Lim SB, *et al*. Signet ring cell component predicts aggressive behaviour in colorectal mucinous adenocarcinoma. Pathology. 2019; 51: 384–391. https://doi.org/10.1016/j.pathol.2019.03.001.